Earthq Eng & Eng Vib (2020) 19: 269-287 **DOI**: https://doi.org/10.1007/s11803-020-0561-2

Influence of random heterogeneity of shear wave velocity on sliding mass response and seismic deformations of earth slopes

Pourya Kazemi Esfeh[1†], Bahram Nadi[2‡] and Nicholas Fantuzzi[1§]

1. *Department of Civil, Chemical, Environmental, and Materials Engineering, University of Bologna, Italy*

2. *Department of Civil Engineering, Azad University of Najafabad, Iran*

Abstract: Soil shear wave velocity has been recognized as a governing parameter in the assessment of the seismic response of slopes. The spatial variability of soil shear wave velocity can influence the seismic response of sliding mass and seismic displacements. However, most analyses of sliding mass response have been carried out by deterministic models. This paper stochastically investigates the effect of random heterogeneity of shear wave velocity of soil on the dynamic response of sliding mass using the correlation matrix decomposition method and Monte Carlo simulation (MCS). The software FLAC 7.0 along with a Matlab code has been utilized for this purpose. The influence of statistical parameters on the seismic response of sliding mass and seismic displacements in earth slopes with different inclinations and stiffnesses subject to various earthquake shakings was investigated. The results indicated that, in general, the random heterogeneity of soil shear modulus can have a notable impact on the sliding mass response and that neglecting this phenomenon could lead to underestimation of sliding deformations.

Keywords: random heterogeneity; random fields; Monte Carlo simulation; sliding mass response; seismic deformations

1 Introduction

Since seismic sliding displacement is a crucial factor for evaluating the seismic stability of slopes, assessment of this factor has been taken into consideration by various researchers and geotechnical professionals over the past few decades. If the sliding mass is rigid (i.e., shallow and stiff sliding mass), the rigid sliding block analysis is appropriate to evaluate the seismic deformation (Newmark, 1965). In this case, the natural period of the sliding mass T_s is very close to zero, and the slope response can be ignored. Thus, the input acceleration time history can be used to estimate the displacement by numerically integrating it over periods where the acceleration is greater than yielding acceleration k_y. The integration process continues for the episodes where the response acceleration drops below k_y until the relative velocity becomes zero. Alternatively, the seismic loading parameters, such as peak ground acceleration (PGA), can be utilized to predict sliding displacements from empirical models. Yielding acceleration is the seismic coefficient corresponding to a unity safety factor that represents the minimum acceleration required to initiate sliding mass failure. However, if the sliding mass is deformable (i.e., deep and soft sliding mass), it has a natural period greater than zero, making rigid sliding block analysis inappropriate. In this case, the seismic response of a deformable sliding mass must be evaluated. One of the most used methods for estimating the dynamic response of sliding mass is the decoupled analysis. In this analysis, seismic response of sliding mass is first computed by ignoring the sliding displacements, and then this computed response is used in a rigid sliding block analysis to estimate displacements (Makdisi and Seed, 1978; Bray and Rathje, 1998). The seismic coefficient time history $k(t)$ is numerically integrated instead of integrating input acceleration time history over periods where the seismic coefficient is higher than yielding acceleration k_y. Alternatively, the maximum seismic coefficient k_{max} is utilized in empirical models instead of PGA to evaluate the seismic displacements.

Soil properties vary in space even within homogeneous soils. However, most geotechnical analyses have been carried out by deterministic models that consider only a mean value of soil parameters applied to a given soil model (e.g., Hui *et al*., 2018; Konai *et al*., 2018; Gu *et al*., 2017; Tang *et al*., 2014, 2016; Gerolymos *et al*., 2009). This simplification leads to the rise of uncertainties (Zhang *et al*., 2019; Jamshidi and Aminzadeh, 2016;

Correspondence to: Nicholas Fantuzzi, Department of Civil, Chemical, Environmental and Materials Engineering, University of Bologna, Viale del Risorgimento, 2, 40136 Bologna, Italy
Tel: +39 051 20 9 3494
E-mail: nicholoas.fantuzzi@unibo.it
[†]Postgraduate; [‡]Assistant Professor; [§]Senior Assisstant Professor
Received January 21, 2019; **Accepted** December 31, 2019

Berkane *et al*., 2014). Indeed, one of the common sources of discrepancy between the estimated and the actual performance of any geotechnical system is the variability of the soil parameters (Phoon and Kulhawy, 1999). Some statistical parameters that represent spatial variability of soil properties include coefficient of variation CoV introduced by mean value and variance, correlation length δ and probability distribution. In recent years, inherent spatial variability and uncertainty of soil properties have received considerable attention. Griffiths *et al*. (2002) studied the effects of spatial variability of undrained shear strength of soil on bearing capacity of rough rigid strip foundations. Haldar and Babu (2008) analyzed the pile bearing capacity under horizontal load considering the heterogeneity of undrained shear strength. In these studies, the Monte Carlo simulation was used to generate random fields. Moreover, the effects of coefficient of variation of undrained shear strength and correlation length on bearing capacity of the pile were interpreted.

A large number of studies have dealt with the influence of spatial variability of soil properties on slope stability and reliability (Hicks and Samy, 2002; Sivakumar Babu and Mukesh, 2003; Griffiths and Fenton, 2004; Low *et al*., 2007; Griffiths *et al*., 2009; Zhang *et al*., 2010; Tietje *et al*., 2014; Metya and Bhattacharya, 2016; Li and Chu, 2016; Deng *et al*., 2017; Liu *et al*., 2017).

Although extensive deterministic numerical studies have been carried out to investigate the dynamic response of slopes (e.g., Liu *et al*., 2019; Huang *et al*., 2018; Tang *et al*., 2017), only a few stochastic studies have examined the uncertainty in evaluating their seismic response. Nadi *et al*. (2014, 2016, 2019) addressed the uncertainty in assessing the seismic slope stability and co-seismic landslide deformations due to the random behavior of soil properties. Lizarraga and Lai (2014) investigated the effects of spatial variability of soil properties on the seismic response of an embankment dam. They studied the impact of the coefficient of variation of cohesion and friction angle, along with the effect of correlation length on maximum crest displacement of an embankment. These researchers concluded that when the aleatory uncertainty of soil characteristics is substantial, the stochastic response of the dam is considerably different from its deterministic response. Michael *et al*. (2016) probed the failure probability in a slope considering shear modulus as a spatially random variable. They computed the failure probabilities regarding different maximum acceleration at the slope toe. Nevertheless, the uncertainty in assessing the seismic response of sliding mass and seismic displacements due to spatial variability of shear wave velocity has not been addressed in the literature.

The sliding mass response (i.e., seismic coefficient *k*-time-history) depends on topographic effects as a result of topographic irregularities and stratigraphic effects due to the heterogeneity of soil shear wave velocity. Considering that stratigraphic effects are connected with shear wave velocity V_s, spatial variability of shear wave velocity leads to different stratigraphic effects and correspondingly different responses of the sliding mass.

This paper investigates the influence of spatial variability of shear wave velocity on the maximum seismic coefficient k_{max} and seismic sliding displacements by generating stationary isotropic random fields. The correlation matrix decomposition method in conjunction with Monte Carlo simulation (MCS) was employed to create random fields of initial shear modulus. Afterward, the dynamic analyses were conducted to evaluate the maximum seismic coefficient k_{max} corresponding to each random field; accordingly, the sliding displacement produced by each maximum seismic coefficient was estimated using a closed-form solution.

The slope models with different inclinations and stiffnesses were used in seismic analyses to gain insight into the way random heterogeneity of shear wave velocity in slopes with different topographic irregularities impacts the total response of sliding mass as stiffness varies with cyclic strain during the earthquake shaking.

2 Deterministic analysis

2.1 Model description

Two typical 2D slope models with the height $H = 20$ m and inclinations $\beta = 30^\circ, 60^\circ$ were considered in dynamic analyses (Fig. 1). The use of slopes with different inclinations gives an insight into the way topographical irregularities influence the seismic sliding mass response. Finite-difference software FLAC 7.0 was employed for performing the dynamic analyses. The model mesh was constructed by extending the lateral boundaries of the model beyond the desired area so that reflected waves would be properly damped, and their influence on the seismic response is minimized. According to Rizzitano *et al*. (2010), the results are not affected by the thickness *B* of the half-space (Fig. 1) provided that the length *L* is long enough to produce a geometrical attenuation of the waves. A sensitivity analysis confirmed that the length $L = 8\ H$ and the thickness $B = 20$ m could be adequate for this end. Additionally, free-field boundary conditions were applied to the left and right sides of the model to reduce the effect of wave reflection.

If the mesh size is not sufficiently small, high-frequency components of the waves may be filtered. The maximum size of elements was determined by using the following expression proposed by Kuhlemeyer and Lysmer (1973) to ensure that all frequency contents of the input motion propagate through the model without compromising the accuracy of the final results.

$$\Delta l \le \frac{V_s}{10 f_{max}} \tag{1}$$

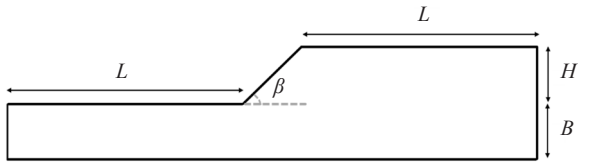

Fig. 1 Geometry of slope model (not to scale)

where Δl is the maximum length of elements and f_{max} is the highest frequency of the input motion. As discussed later, the minimum mean shear wave velocity assigned to the model is equal to 250 m/s, and the maximum frequency contents of all ground motions applied to the slope models do not exceed 12 Hz. Therefore, if constructing the model by square elements with length Δl = 2 m, the criterion in Eq. (1) is respected by all seismic input motions used in the present study. Two grids of 177 by 20 zones and 166 by 20 zones (2 m by 2 m size) with geometrical features discussed earlier were generated to represent the slopes with angles $\beta = 30^\circ$ and $\beta = 60^\circ$.

The density ρ = 2000 kg/m^3 along with Poisson′s ratio v = 0.3 was assigned to the soil and held constant in all analyses. The Mohr-Coulomb constitutive model with strength parameters of cohesion c = 25 kPa and friction angle $\phi = 35^\circ$ was assigned to the soil. These strength parameters were selected so that both slopes inclining at $\beta = 30^\circ$ and $\beta = 60^\circ$ would be statically stable. These parameters influence the seismic response of sliding mass only if the yield stress is reached during the earthquake; nonetheless, the soil stiffness (defined by shear wave velocity) is the governing soil parameter, which has a major influence on results of nonlinear time-domain analyses and the dynamic response of sliding mass. Spatial variations in shear wave velocity lead to the changes in natural period of sliding mass, thereby remarkably influencing the maximum seismic coefficient when the natural period of sliding mass approaches the mean period of input motion (explained in section 4.1 in detail). Moreover, spatial variability of strength parameters could result in diverse slip surface geometries in each random field, thereby making it hard to detect the failure mechanism and to determine the average response acceleration along the slip surface. Therefore, strength parameters were kept constant for all models, and the spatial variability of shear modulus was simulated using random fields. Two mean initial shear moduli G_0 = 125 MPa and G_0 = 320 MPa related to shear wave velocities V_s = 250 m/s and V_s = 400 m/s by the following equation were assigned to the soil to study the seismic response of sliding masses with different stiffnesses. Initial shear modulus and shear wave velocity are related by

$$G_0 = \rho V_s^2 \tag{2}$$

The considered shear wave velocities fall within the most common values of this parameter used in the literature (for instance, Bray and Rathje, 1998; Michael *et al*., 2016).

The numerical model was verified with an analytical solution for assessing the dynamic amplification factor A associated with a homogeneous linear-elastic soil medium as

$$A = \frac{1}{\sqrt{\cos^2\left(\frac{\omega H}{V_s}\right) + \left(\xi \frac{\omega H}{V_s}\right)^2}} \tag{3}$$

where ω and ξ are the angular frequency of the wave and damping ratio. A soil deposit with the height H = 40 m, length L=354 m and V_s = 250 m/s was modeled with the square elements of length Δl = 2 m (grid of 177 by 20 zones) and subjected to harmonic loads with the amplitude of 0.1 g and frequencies ($f = \omega/2\pi$) varying from 0 to 12 Hz. Moreover, the damping ratio ξ = 3% was considered as explained in the next section. Numerically computed amplification factors fit very well with those resulting from the analytical solution confirming that boundary conditions and element sizes are adequately determined (see Fig. 5(a)).

2.2 Damping

Fully non-linear codes such as FLAC 7.0 are capable of reproducing energy dissipation inherently with elasto-plastic constitutive models. Since Mohr-Coulomb constitutive law is assigned to the soil, damping is automatically generated within only the plastic range. Anyway, the Mohr-Coulomb model cannot reproduce proper energy dissipation and shear modulus reduction in elastic range since it has a constant tangent elastic shear modulus, and yield stress. Therefore, in conjunction with the Mohr-Coulomb model, additional damping must be included to account for energy dissipation during the elastic range. Typically, hysteretic damping is used to simulate strain-dependent shear modulus and damping within the elastic range. Using hysteretic damping is questionable if large cyclic shear strains occur since it leads to a significant shear modulus reduction giving on to irrelevant seismic response amplitudes. Preliminary dynamic analyses showed that the maximum level of cyclic shear strain developed within undamped elastic slopes subjected to input motions with high levels of PGA was large enough to cause considerable shear modulus reductions and unrealistic seismic responses. Since one of the principal objectives of this study is to assess the dynamic response of slopes subjected to a broad range of earthquake shakings, it is not viable to use input motions with merely average amplitudes to reduce the cyclic shear strain. Therefore, considering hysteretic damping for this study is not a wise choice.

Moreover, the presence of soft elements in the random fields with low shear modulus gives rise to difficulties

in using hysteretic damping since a further reduction of shear modulus in these elements leads to unrealistic seismic responses. Alternatively, the Rayleigh damping was used although it is frequency-independent merely for a limited span of frequencies. Rayleigh damping matrix is composed of the components proportional to the mass and stiffness matrices through the coefficients α and β. These coefficients could be defined in a way to achieve the frequency-independent damping. To this end, the center frequency is chosen to lie between either natural frequencies of the model or predominant frequencies of the input motion. In this study, the critical damping ratio ξ = 3% at the mean frequency of input motion was considered. This amount of damping ratio is deemed to be sufficient to damp the energy and also to minimize the possible over-damping occurring beyond the range of predominant frequencies.

2.3 Input motions

Six significant earthquake records having different characteristics occurred in north and east parts of Iran (IIEES, International Institute of Earthquake Engineering and Seismology) were designated for this study (Table 1). Peak ground accelerations (PGA) range from 0.085 g to 0.531 g, mean periods T_m (Rathje *et al*., 1998) range from 0.137 s to 0.785 s and effective durations range from 4 s to 25 s. Baseline correction was performed for all earthquake records. Since frequency contents of earthquake records do not exceed 12 Hz that is utterly compatible with the smallest size of mesh elements, these records were not filtered.

2.4 Slip surface geometry and yielding acceleration

The pseudo-static analysis was carried out to determine the critical slip surface geometry and the yielding acceleration k_y. Yielding acceleration is the seismic coefficient corresponding to a unity safety factor which represents the minimum acceleration required to initiate a sliding mass failure. This parameter indicates the slope resistance against the horizontal force of an earthquake and depends upon the strength parameters of soil and slope geometry. It is a crucial parameter for assessing the sliding displacements as addressed later. Having performed multistep pseudo-static analyses, the horizontal acceleration was incrementally increased up to the value for which the safety factor reached one, and the sliding mass was on the verge of failure. It is worth noting that the vertical component of the acceleration (vertical force of the earthquake) was not considered in these analyses. Yielding accelerations k_y = 0.41 and k_y = 0.13 were estimated for the slopes of interest with inclinations $\beta = 30^\circ$ and $\beta = 60^\circ$ respectively. Furthermore, detecting the slip surface geometry is required to evaluate k_{max} as explained in section 2.5. To determine the slip surface geometry, the coordinates of points at which maximum shear strain increment (ssi) was equal or more than 70% of the peak strain value were specified using a FISH function. Levenberg-Marquardt Least-Square method was used to fit the best circular curve to the stated points. Figure 2 indicates the detected slip surface for the slope with inclination $\beta = 30^\circ$.

2.5 Maximum seismic coefficient

The seismic coefficient time history was evaluated by computing the average response acceleration time history on the slip surface using a FISH function. The sliding mass was divided into blocks with equal widths, and the response acceleration at the bottom-center point of each block, located on the slip surface, was computed. Consequently, seismic coefficient time history $k(t)$ was evaluated as a weighted average of the response accelerations at these points at each time step as

$$k(t) = \frac{\sum_{i=1}^{n} a_i(t) m_i}{m} \tag{4}$$

where $a_i(t)$, m_i and m are the acceleration time history at each bottom-center point i located on slip surface, the mass of ith block and total sliding mass. The k-time history represents the dynamic response of sliding mass whose maximum absolute value is known as the maximum seismic coefficient k_{max}.

2.6 Seismic sliding displacements

Decoupled sliding block analysis can be employed to estimate the seismic sliding displacements of a deformable sliding mass by integrating k-time history over the periods k values exceed k_y. This approximation is

Table 1 Characteristics of input motions

No.	Location-station	PGA (m/s^2)	T_m (s)	M	Effective duration (s)
1	Bandarabas-bandarabas	0.84	0.402	6.1	16
2	Qaen-khezri	0.99	0.785	7.1	15
3	Qaen-bajestan	1.14	0.304	7.1	13
4	Tularud-talesh	2.31	0.242	6	7
5	Kajoor-hasan keyf	4.42	0.357	6.3	4
6	Eslamabad-kariq	5.21	0.137	6	5

termed 'decoupled' since the dynamic response analysis is performed decoupled from sliding block analysis. Alternatively, k_{max} can be used in empirical formulae for computing sliding displacements. Since this study investigates the effect of random heterogeneity of shear modulus on the maximum seismic coefficient k_{max} as a seismic loading parameter commonly used in empirical formulae, a predictive model has been employed for computing the sliding displacements rather than integrating the entire seismic coefficient time history $k(t)$. Indeed, the main goal was to investigate how the deviation of k_{max} from its deterministic value arising from spatial variability of shear wave velocity could impact the seismic deformations obtained by empirical formulae. It is worth noting that the use of multiple ground motions to characterize the earthquake shaking and incorporation of various earthquake parameters to these predictive models have significantly improved their precision (Rathje and Saygili, 2011). Seismic sliding displacements in the present study are estimated by the following expression suggested by Rathje and Saygili (2011).

$$\ln(D) = a_1 + a_2\left(\frac{k_y}{k_{max}}\right) + a_3\left(\frac{k_y}{k_{max}}\right)^2 + a_4\left(\frac{k_y}{k_{max}}\right)^3 + a_5\left(\frac{k_y}{k_{max}}\right)^4 + a_6\ln(k_{max}) + a_7(M-6) + f_1(T_s)$$

with

$$f_1(T_s) = \begin{cases} 3.69T_s - 1.22T_s^2, & T_s \le 1.5\ \text{s} \\ 2.78, & T_s > 1.5\ \text{s} \end{cases} \quad (5)$$

where D, M, and T_s are seismic sliding displacement, the magnitude of the earthquake and natural period of sliding mass, respectively. Parameters a_1 to a_7 are summarized in Table 2. The natural period of sliding mass T_s can be estimated by various expressions proposed by different researchers. In the present study, T_s is defined by the following equation proposed by Makdisi and Seed (1978).

$$T_s = \frac{4y}{V_s} \quad (6)$$

where y is the maximum depth of sliding mass. Four values of T_s are obtained based on soil shear wave velocity and the maximum depth of sliding mass as reported in Table 3.

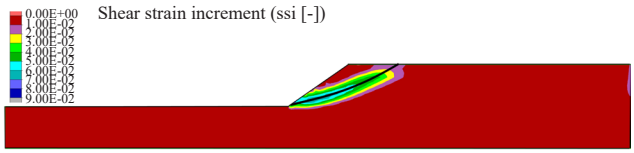

Fig. 2 Slip surface geometry and shear strain increment (ssi) contour resulting from pseudo-static analysis for the slope with $\beta = 30^\circ$

3 Stochastic analysis

3.1 Random field model

One of the primary sources of uncertainty in geotechnical analyses is the spatial variability of soil properties. The characteristics of soil can change from one point to another even if the soil is homogeneous. Therefore, the effect of spatial variability of soil characteristics on the response of soil structures must be carefully addressed in order to reduce the uncertainty. Since soil stiffness is the most significant soil characteristic influencing the seismic response of sliding mass, the spatial variability of shear modulus was simulated by random field generation while strength parameters were kept constant as explained in section 2.1. The shear wave velocities were related to the initial shear moduli using Eq. (2), and the random fields of initial shear modulus were generated as described in the following. The random variation of initial shear modulus G_0 was modeled by the lognormal distribution with three key parameters: mean μ_{G0}, standard deviation σ_{G0} and correlation length δ. The reason behind characterizing

Table 2 Parameters of Eq. (5) (Rathje and Saygili, 2011)

Parameters	
a_1	4.89
a_2	-4.85
a_3	-19.64
a_4	42.49
a_5	-29.06
a_6	0.72
a_7	0.89

Table 3 Natural periods of sliding masses in different slopes

Slope angle	$\beta = 30^\circ$		$\beta = 60^\circ$	
Shear wave velocity V_s (m/s)	250	400	250	400
Maximum thickness of sliding mass (m)	11.606	11.606	11.43	11.43
Natural period of sliding mass (s)	0.185	0.116	0.182	0.114

shear modulus by the lognormal distribution is that based on experimental studies (Cherubini, 2000; Baecher and Christian, 2003), soil properties follow normal (Gaussian) or lognormal distributions. Furthermore, considering that soil shear modulus cannot be negative, the use of lognormal distribution could be appropriate as it owns only positive values.

The correlation length δ indicates the distance over which the spatially random values tend to be correlated. Correlation length δ is normalized by slope height H, and the standard deviation is expressed in terms of the coefficient of variation $\mathrm{CoV}_{G0}= \sigma_{G0}/\mu_{G0}$. Table 4 lists the probabilistic parameters used in this study.

The generated random fields in this study are characterized as non-Gaussian isotropic random fields since the random shear moduli are produced by the (non-Gaussian) lognormal probability distribution and horizontal and vertical correlation lengths are deemed to be equal (i.e., $\delta_h = \delta_v = \delta$). Besides, these random fields are stationary as they have all the following features:

(1) Mean initial shear modulus μ_{G0} and its standard deviation σ_{G0} are constant for all depths.

(2) The spatial correlation of each two points does not depend on their absolute locations but the distance between them.

(3) The probability distribution function is independent of the absolute locations.

The use of isotropic stationary random fields simplifies the problem, and it is sufficient to study the basic stochastic seismic response of sliding mass and sliding deformations. The effects of anisotropic or non-stationary variability of shear wave velocity on the dynamic response of sliding mass are left for future studies.

3.2 Random field generation

A correlation matrix $\boldsymbol{C}$ was generated using an isotropic Markovian spatial correlation function as

$$\rho(\tau) = \exp\left(-\frac{2\tau}{\delta}\right) \tag{7}$$

where ρ, τ and δ are respectively the correlation coefficient, the distance between any two consecutive points of the desired random field and the correlation length. The correlation matrix $\boldsymbol{C}$ represents the inherent spatial correlation between the points and has the form

$$\boldsymbol{C} = \begin{bmatrix} c_{11} & c_{12} & \cdots & c_{1n} \\ c_{21} & c_{22} & \cdots & c_{2n} \\ \vdots & \vdots & \ddots & \vdots \\ c_{n1} & c_{n2} & \cdots & c_{nn} \end{bmatrix} \tag{8}$$

where the element c_{ij} is equal to the correlation coefficient ρ corresponding to the points i and j. The spatial correlation of each point with itself is equal to one; hence, diagonal elements c_{ij} are equal to unity. Figure 3 depicts a discretization of the finite difference grid of the slope model with inclination $\beta = 30^\circ$ based on which the correlation matrix $\boldsymbol{C}$ is formed. As demonstrated in this figure, d_x and d_y are the horizontal and vertical distances between two adjacent points. As model mesh elements are square elements with the length $\Delta l = 2$ m, $d_x = d_y = 2$ m. Accordingly, the distance τ between all the points can be computed using d_x and d_y. A code was created in Matlab to generate matrix $\boldsymbol{C}$ according to Eq. (8). The matrix $\boldsymbol{C}$ is a symmetrical square matrix of dimension n where n is the number of mesh elements in the finite-difference model. Grids of 177 by 20 zones and 166 by 20 zones (2 m by 2 m size) were used for dynamic simulations of slopes with inclinations

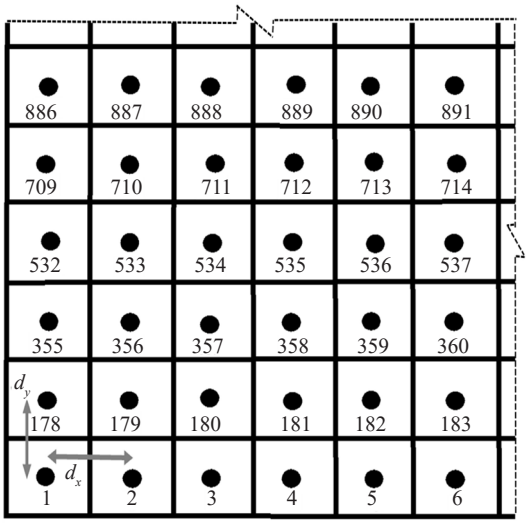

Fig. 3 Discretization of finite difference grid

Table 4 Ranges of stochastic parameters for initial shear modulus/shear wave velocity

Stochastic parameters	Value
Mean shear wave velocity, V_s (m/s)	250, 400
Mean shear modulus, μ_{G0} (MPa)	125, 320
Coefficient of variation, CoV_{G0} (%)	13, 30
correlation length, δ (m)	4, 8, 16, 40, 100, 200
Normalized correlation length, δ/H	0.2, 0.4, 0.8, 2, 5, 10

β = 30˚ and β = 60˚. Thus, matrix $\boldsymbol{C}$ is a symmetrical matrix of size 3540 for the slope model inclined at 30˚ and of size 3320 for the slope model inclined at 60˚. The correlation coefficient decreases as the distance between two points increases indicating that the soil properties at every two points of the model become less spatially correlated as the distance between them increases. The correlation matrix $\boldsymbol{C}$, which is a positive definite matrix, was decomposed into a lower matrix $\boldsymbol{L}$ and its transpose using Cholesky decomposition,

$$\boldsymbol{C} = \boldsymbol{L}\boldsymbol{L}^{\mathrm{T}} \tag{9}$$

The normal standard random field $G(x_i)$ was formed by multiplication of the matrix $\boldsymbol{L}$ by a sequence of independent standard random variables with zero mean and unit standard deviation. Consequently, a lognormally random field of initial shear modulus was generated by

$$G_{0_{\mathrm{i}}} = \exp\left\{\mu_{\ln G_0} + \sigma_{\ln G_0} \cdot G\left(x_i\right)\right\} \tag{10}$$

where x_i is the center position of the ith element at which the initial shear modulus $G_{0\mathrm{i}}$ is desired.

The parameters $\mu_{\ln G0}$ and $\sigma_{\ln G0}$ were obtained by lognormal distribution transformations given by the following equations.

$$\sigma^2_{\ln G_0} = \ln\left(1 + \frac{\sigma^2_{G_0}}{\mu^2_{G_0}}\right) = \ln(1 + \mathrm{CoV}^2_{G_0}) \tag{11}$$

$$\mu_{\ln G_0} = \ln G_0 - \frac{1}{2}\sigma^2_{\ln G_0} \tag{12}$$

3.3 Monte Carlo simulation

Monte Carlo simulations were performed for each set of statistical parameters including CoV_{G0} and δ/H as summarized in Table 4. According to Der Kiureghian and Ke (1988), to obtain accurate results, the element size in a random field must be one-quarter to one-half of the scale of fluctuation (i.e., 2 × correlation length δ). In this study, the random field mesh is the same size as the finite element mesh (with the same number of elements); therefore, the element size in the random field is equal to 2 m. According to the stated criterion, if correlation length δ = 4 m (i.e., the scale of fluctuation = 8 m) is considered as the minimum value of this parameter for stochastic analyses, the element size must be 2 m to 4 m in order to assure the accuracy of the results which is consistent with the element size in the random field (the same values were reported by Lizzaraga and Lai (2014)). Investigating the effect of the spatial variation of shear wave velocity with $\delta = 2H$ (i.e., total height of slope) is of particular interest since, as reported in previous studies (e.g., Griffiths *et al*., 2002; Haldar and Babu, 2008), the structure could be sensitive to the fluctuation of soil properties when the correlation length lies within the size of structure (in this case, total height of slope). The correlation length δ = 10 H was chosen to have insight into the variation of maximum seismic coefficient when the correlation length increases to large values and accordingly, the random field becomes more homogeneous. The coefficients of variation CoV_{G0} were chosen to fall within the most typical values reported in the literature (e.g., Jamshidi *et al*., 2012; Kim and Santamarina, 2017).

Monte Carlo simulations were performed considering the aforementioned statistical parameters for slope models with different initial shear moduli and inclinations. To this end, a Matlab script was written and the random fields were generated as described earlier. Random field meshes of initial shear modulus were mapped to the finite difference meshes of slopes by assigning each initial shear modulus of the random field to its corresponding finite difference element using a FISH function embedded in the main FLAC code. For each set of statistical parameters, 700 realizations of initial shear modulus random field were generated and the dynamic analysis corresponding to each random field was carried out. Subsequently, the maximum seismic coefficient $k_{\max}$ was evaluated in each dynamic simulation and the sliding displacement D was estimated using Eq. (5). Despite having the same statistical characteristics, realizations have entirely different spatial patterns of initial shear modulus. Therefore, different values of the maximum seismic coefficient $k_{\max}$ and sliding displacement D have resulted from each realization.

As a result of the random nature of realizations, estimated values of the maximum seismic coefficient $k_{\max}$ fluctuate remarkably, and it accordingly leads to the fluctuation of sliding displacements D. Thus, the number of generated realizations must be large enough to limit the fluctuation of outputs and to obtain stable/accurate statistics of $k_{\max}$ and D. Figure 4 illustrates the fluctuation of mean and coefficient of variation of $k_{\max}$ and D with the number of realizations regarding the dynamic analysis with earthquake record No.1, mean initial shear modulus μ_{G0} =125 MPa, β = 60˚, CoV_{G0}=13% and δ/H = 0.2. This figure shows that the fluctuation of statistics of $k_{\max}$ and D significantly decreases as the number of realizations escalates and falls in a tolerable range with 700 realizations, as considered in this study.

4 Results and discussions

4.1 Results of deterministic analyses

The performance of the numerical model was verified with the closed-form solution for computing the dynamic amplification factor in a homogeneous linear-elastic soil medium as discussed earlier. Figure 5(a)

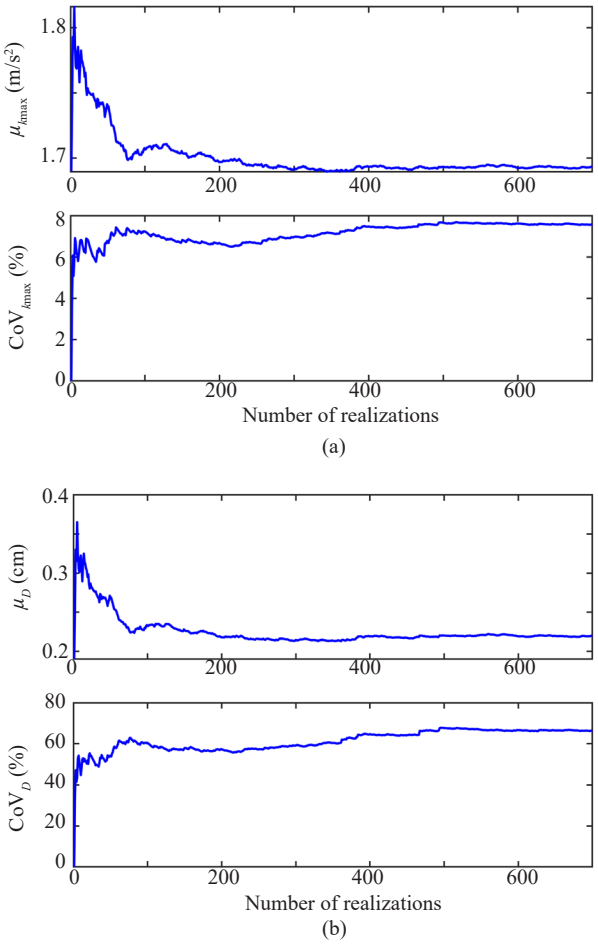

Fig. 4 Mean and coefficient of variation of (a) maximum seismic coefficient and (b) sliding displacement as function of number of realizations

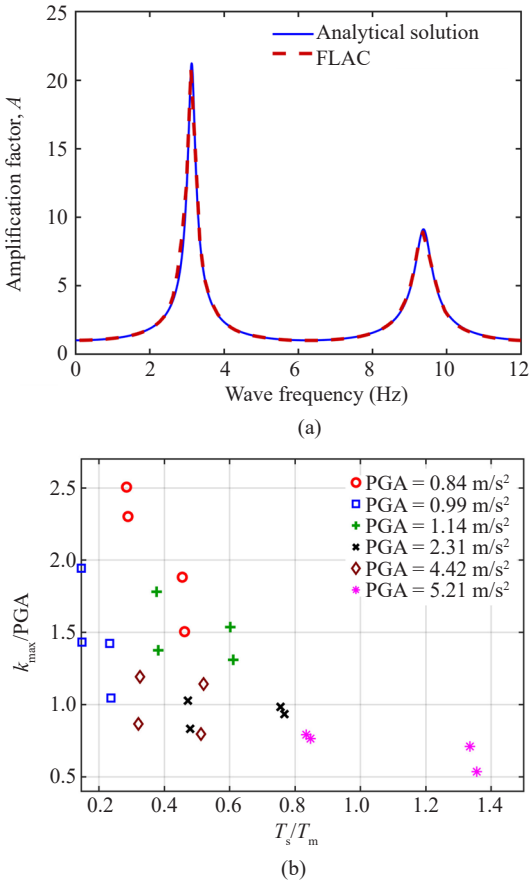

Fig. 5 (a) Comparison of analytically and numerically computed dynamic amplification factor in the homogeneous linear-elastic soil medium; (b) Variation of deterministic k_{max}/PGA versus T_s/T_m

compares the numerically and analytically computed amplification factors confirming that the numerical model consistently simulates the dynamic response of the homogeneous linear-elastic soil medium.

Deterministic seismic analyses were carried out for slopes inclined at β = 30˚ and β = 60˚ assigning fixed values of initial shear modulus G_0 = 125 MPa and G_0 = 320 MPa to the soil. Figure 5(b) indicates the variation of k_{max}/PGA with period ratio T_s/T_m (i.e., the natural period of sliding mass over the mean period of input motion) for various levels of PGA. It can be observed that k_{max}/PGA values greater than one correspond to the moderate period ratios (i.e., T_s/T_m = 0.1 to 0.8), whereas these values are less than one at greater period ratios. In other words, dynamic response amplification could occur in the range of moderate period ratios while dynamic response de-amplification takes place beyond this range. Moreover, it can be concluded that k_{max}/PGA decreases as PGA increases. The same results were reported by Rathje and Antonakos (2010).

Table 5 lists the deterministic values of k_{max}/PGA and D regarding the slope models with β = 30˚ and β = 60˚. Based on the statistics of this table, the values of k_{max}/PGA are generally higher in slopes with β = 60˚ than those in slopes with β = 30˚. The reason for this discrepancy is the effect of slope inclination on topographic amplification that correspondingly influences the total amplification. In general, the topographic amplification influences the total dynamic response more significantly as the slope inclination increases (Bouckovalas and Papadimitriou 2005). The other key factor influencing total dynamic response is the stratigraphic amplification depending on the natural period of sliding mass T_s which is a function of shear wave velocity of the soil V_s. According to Eq. (2), an increase in V_s leads to a decrease in T_s so that T_s/T_m gets closer to intermediate values. Thus, as listed in Table 5, for low values of PGA, k_{max}/PGA escalates as an increase in V_s from 250 m/s (μ_{G0} =125 MPa) to 400 m/s (μ_{G0}= 320 MPa). Sliding displacements in slopes with β = 30˚ are equal to zero for almost all seismic input motions since k_y values associated with these slopes are high enough to prevent sliding displacements.

4.2 Results of stochastic analyses

The range of variation of shear modulus within a

random field is defined by CoV_{G0}, the greater the CoV_{G0}, the higher the variation of initial shear modulus. Figure 6 demonstrates a plot of generated random fields with different statistical characteristics. As shown in Figs. 6 (a) and (b), when CoV_{G0}=13% and δ/H = 0.2, initial shear moduli vary from 90 MPa to 160 MPa while for the same δ/H and CoV_{G0} = 30%, they vary within a wider range (i.e., from 50 MPa to 200 MPa). Furthermore, it can be observed that an increase in CoV_{G0} leads to a rise in the number of soft elements (with low initial shear moduli) in the random field.

The homogeneity of a random field is represented by δ/H. This parameter indicates how homogeneous, or erratic, a random field is. If δ/H is small, the initial shear modulus varies rapidly from one element to another generating an erratic random field (Fig. 6(b)). On the contrary, for large δ/H, initial shear modulus changes slowly creating a more homogeneous random field (Fig. 6(c)).

Figures 7-10 display the variation of μ_{kmax}/PGA with δ/H and CoV_{G0} for various slope models. In general, the ratio μ_{kmax}/PGA increases with CoV_{G0}. The reason is that an increase in CoV_{G0} results in a higher number of stiff elements (with high initial shear moduli) in the random field and it correspondingly causes a decrease in the natural period of sliding mass T_s according to Eq. (6). Consequently, a lower value of T_s (lower T_s/T_m) results in a higher value of μ_{kmax}/PGA (see Fig. 5(b)). As concluded from the results of deterministic analyses, μ_{kmax}/PGA decreases for higher values of PGA, and it appears that even the presence of stiffer elements as a result of higher CoV_{G0} does not increase the ratio μ_{kmax}/PGA in these cases. For instance, as shown in Figs. 7-10, an increase in CoV_{G0} from 13% to 30% does not lead to a remarkable increase in the ratio μ_{kmax}/PGA for earthquake records No. 5 and No. 6 with high levels of PGA.

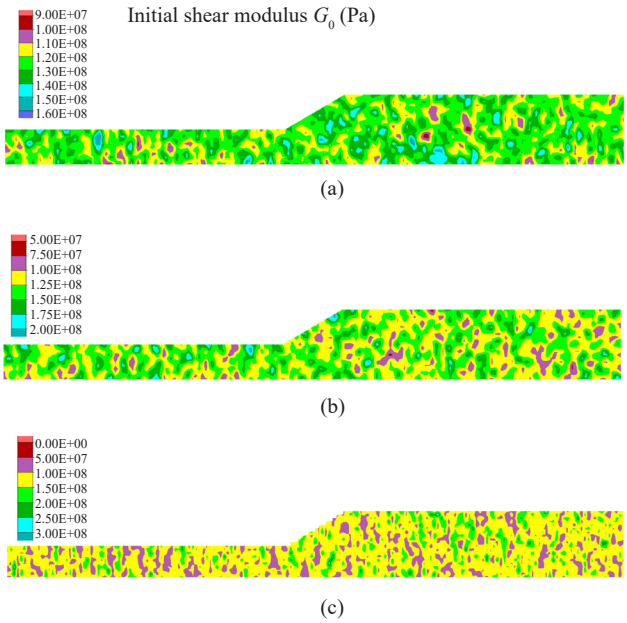

Fig. 6 A realization of random field with μ_{G0} = 125 MPa and (a) CoV_{G0} = 13% and δ/H = 0.2 (b) CoV_{G0} = 30% and δ/H = 0.2 (c) CoV_{G0} = 30% and δ/H = 0.8

The deterministic value of k_{max}/PGA for the slope model with β = 30° and μ_{G0} =125 MPa subjected to the earthquake shaking No. 1 is about 1.5 while the corresponding stochastic μ_{kmax}/PGA rises to 2.3 (i.e., 53% higher than the deterministic one) if the initial shear modulus varies with CoV_{G0} = 30% and δ/H = 2 within the same slope model (see Fig. 7). If the earthquake shaking No. 6 is applied to the same model, the deterministic k_{max}/PGA is estimated as 0.54, whereas the stochastic μ_{kmax}/PGA is only 12% higher than the deterministic one (see Fig. 7). It indicates that the influence of CoV_{G0} on the dynamic response of a sliding mass under seismic input motions with high values of PGA is less significant. In general, it can be concluded that stiffer elements dominate the total seismic response of sliding mass in particular for ground shakings with low levels of PGA.

At lower values of δ/H, the ratio μ_{kmax}/PGA is noticeably smaller. The reason behind this phenomenon is that at low values of δ/H, soft elements are located close to the stiffer elements, producing a rapid change in shear modulus. This rapid change from stiffer to softer elements limits the amplification of acceleration along the slip surface, and accordingly, the maximum seismic coefficient diminishes, since the seismic coefficient is the average of response accelerations along the slip surface. It is speculated that softer elements adjacent to stiffer ones neutralize the effect of stiffer elements on amplification of acceleration. For instance, having a closer look at Fig. 7 reveals that for earthquake shaking No. 1 and CoV_{G0} = 30%, μ_{kmax}/PGA is about 1.76 (i.e., the minimum value of μ_{kmax}/PGA for CoV_{G0}= 30%) at lowest value of δ/H (i.e., δ/H = 0.2), while it increases up to 2.3 as correlation length δ increases to two times the slope height H. The explanation lies in the fact that when the correlation length increases, the random field becomes smoother such that stiffer elements are formed further from softer elements. Therefore, it leads to a higher amplification of average acceleration along the slip surface due to the absence of softer zones adjacent to stiffer ones. For δ/H ratios higher than two where the random field becomes more homogenous, the rate of changes in μ_{kmax}/PGA declines noticeably. It can be concluded that in almost all cases the highest value of μ_{kmax}/PGA corresponds to δ/H = 2, which could be considered as the critical correlation length. In other words, when the correlation length is equal to the total height of slope (i.e., $H+B = 2H$), the seismic response of sliding mass is considerably affected by the variation of initial shear modulus.

Figures 11 and 12 illustrate the variation of mean sliding displacement with δ/H and CoV_{G0} for slope models with β = 60°. As discussed earlier, the sliding displacements in slopes inclined at β = 30° are small/zero due to high values of yielding acceleration k_y in these slopes. Therefore, even high levels of the maximum

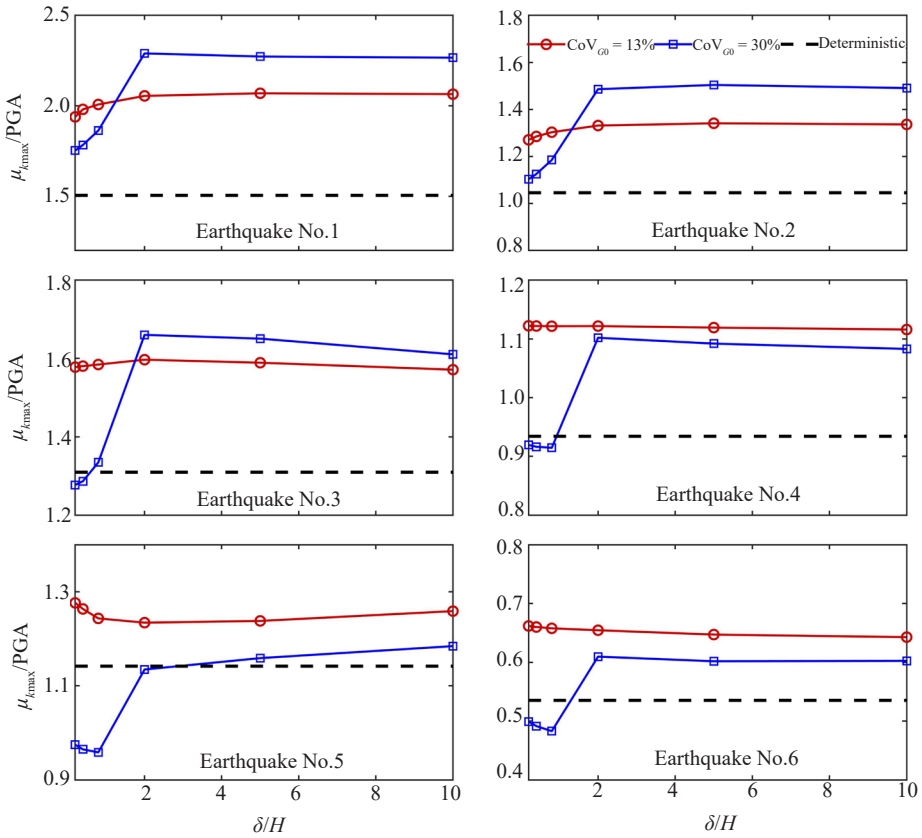

Fig. 7 Variation of mean maximum seismic coefficient with CoV$_{G0}$ and δ/H for the slope model with $\beta = 30^\circ$ and mean initial shear modulus $\mu_{G0} = 125$ MPa

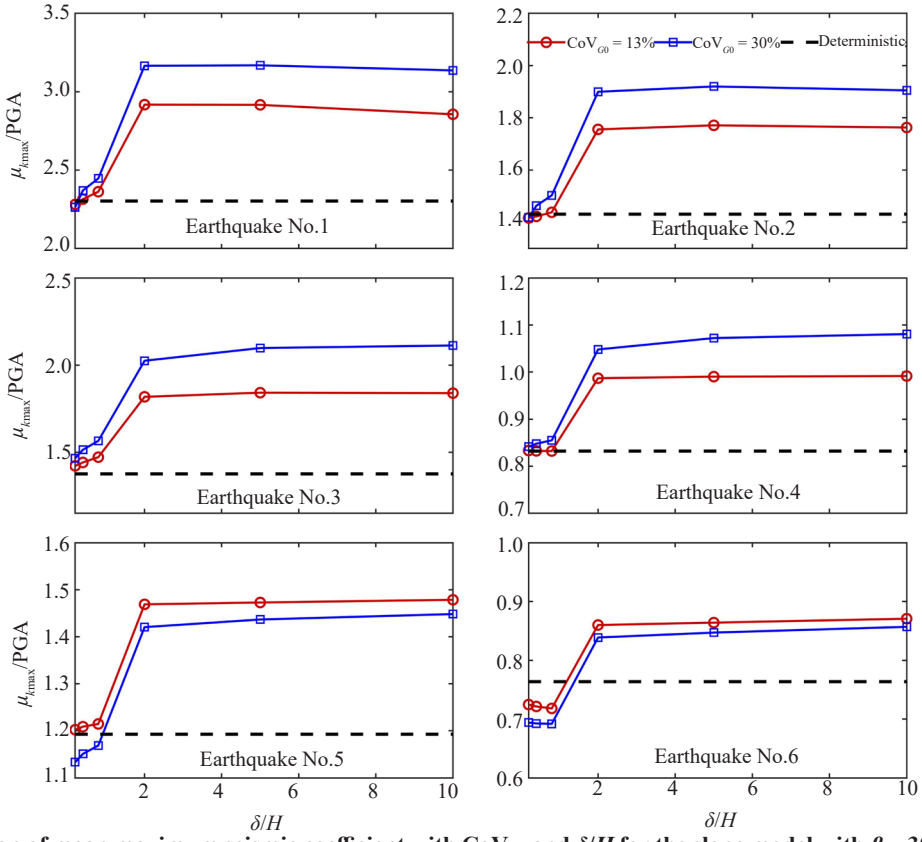

Fig. 8 Variation of mean maximum seismic coefficient with CoV$_{G0}$ and δ/H for the slope model with $\beta = 30^\circ$ and mean initial shear modulus $\mu_{G0} = 320$ MPa

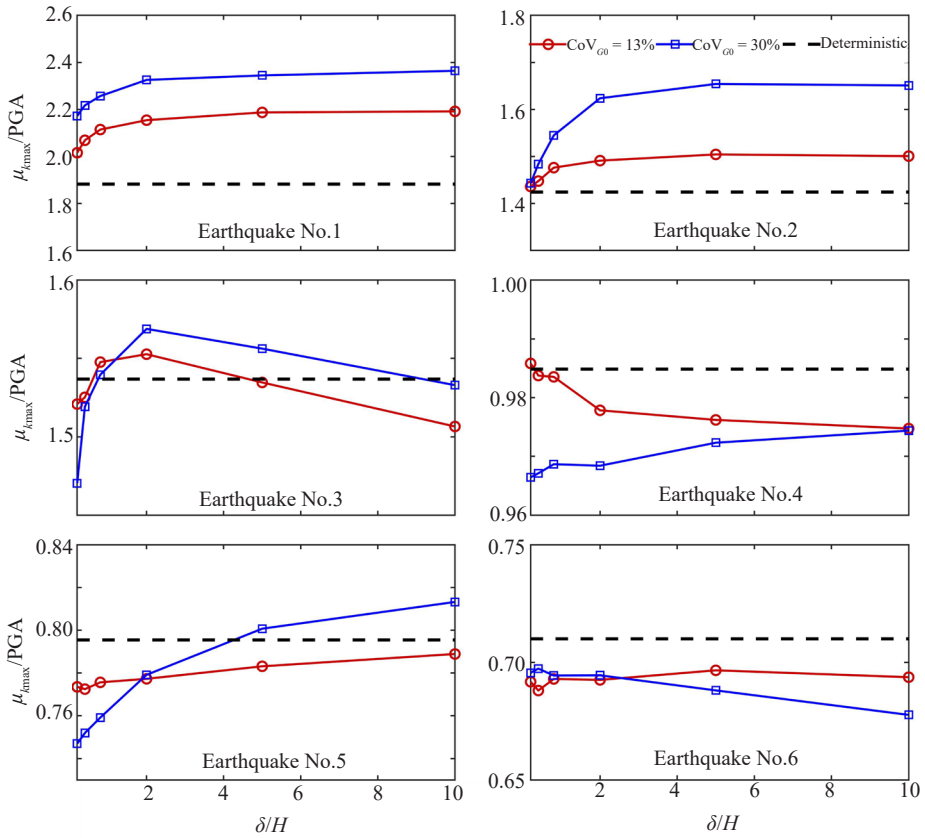

Fig. 9 Variation of mean maximum seismic coefficient with CoV$_{G0}$ and δ/H for the slope model with $\beta = 60^\circ$ and mean initial shear modulus $\mu_{G0} = 125$ MPa

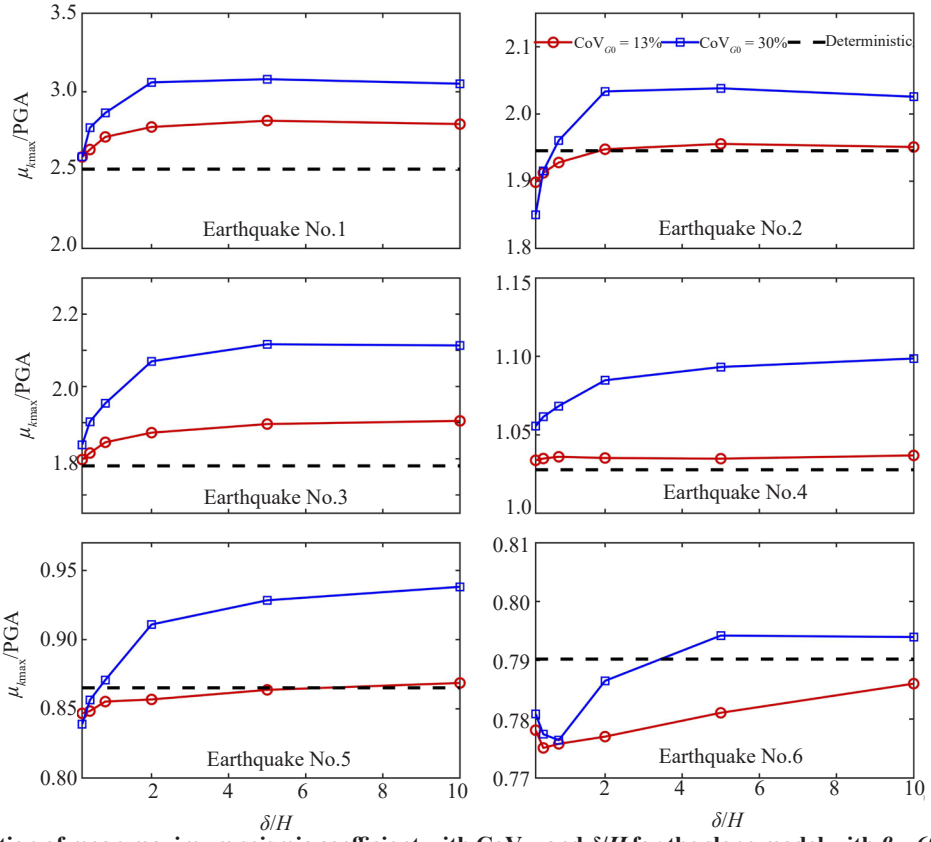

Fig. 10 Variation of mean maximum seismic coefficient with CoV$_{G0}$ and δ/H for the slope model with $\beta = 60^\circ$ and mean initial shear modulus $\mu_{G0} = 320$ MPa

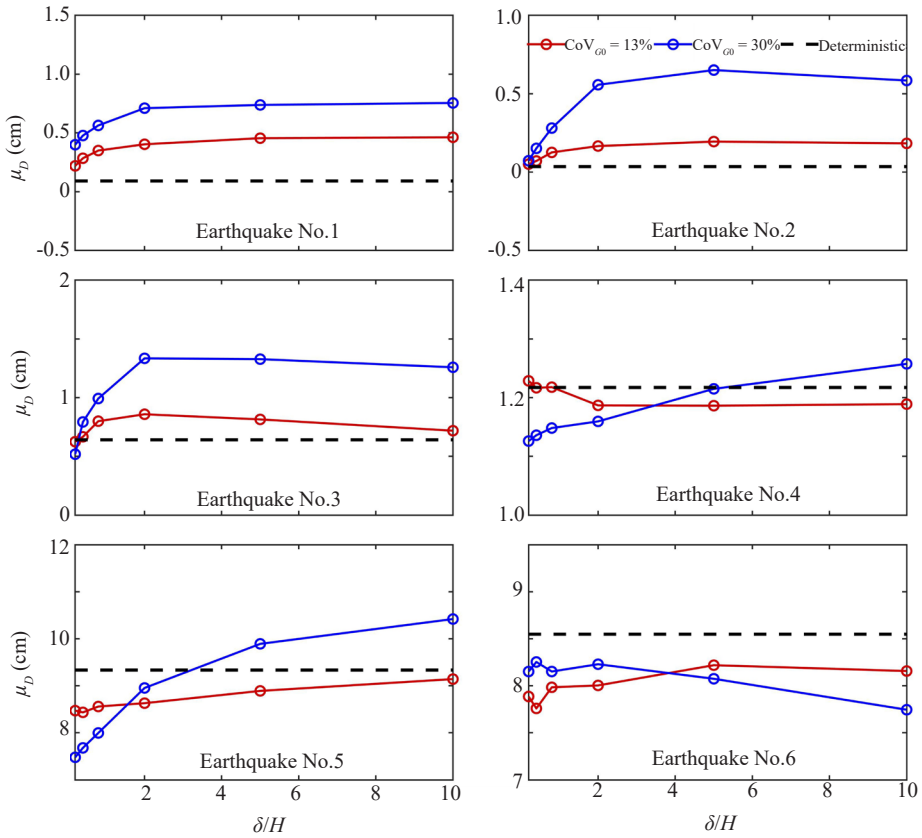

Fig. 11 Variation of mean sliding displacement with CoV$_{G0}$ and δ/H for the slope model with β = 60° and mean initial shear modulus μ_{G0} = 125 MPa

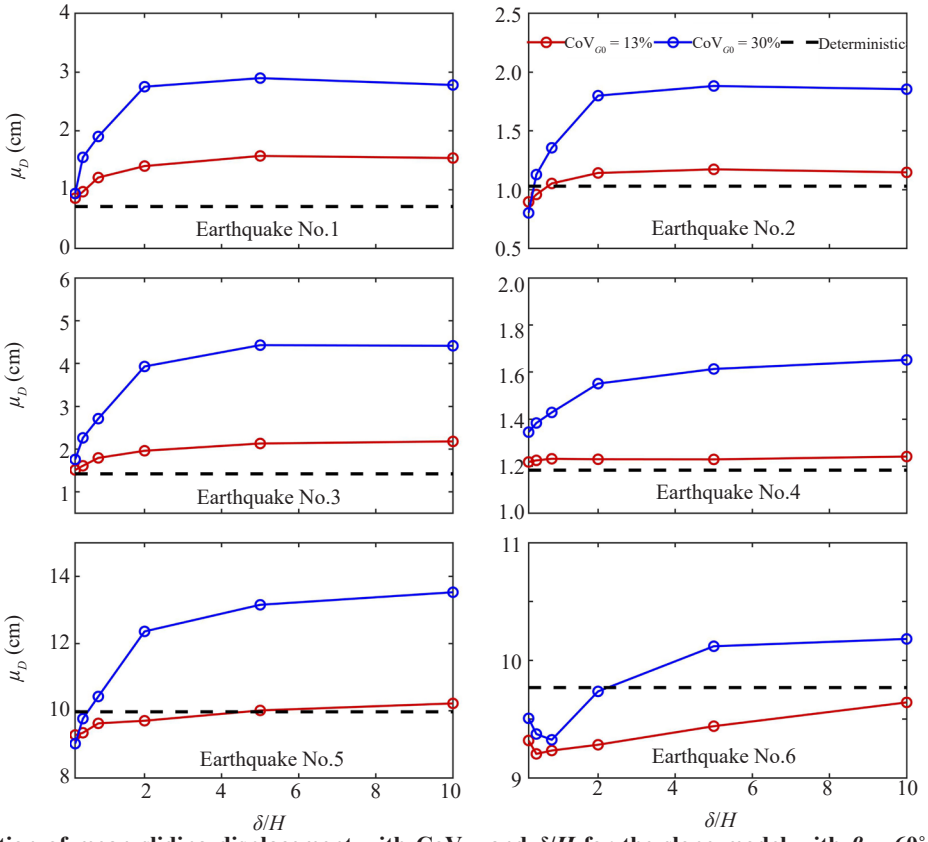

Fig. 12 Variation of mean sliding displacement with CoV$_{G0}$ and δ/H for the slope model with β = 60° and mean initial shear modulus μ_{G0} = 320 MPa

Table 5 A summary of results of deterministic analyses

Slope angle	$\beta = 30^\circ$				$\beta = 60^\circ$			
Deterministic value	k_{max}/PGA		D (cm)		k_{max}/PGA		D (cm)	
μ_{G0} (MPa)	125	320	125	320	125	320	125	320
Earthquake No.1	1.50	2.30	0	0	1.88	2.51	0.091	0.714
Earthquake No.2	1.05	1.43	0	0	1.42	1.95	0.035	1.030
Earthquake No.3	1.31	1.38	0	0	1.54	1.78	0.641	1.420
Earthquake No.4	0.93	0.83	0	0	0.98	1.03	1.217	1.183
Earthquake No.5	1.14	1.19	0.29	0.37	0.80	0.87	9.336	9.966
Earthquake No.6	0.54	0.76	0	0	0.71	0.79	8.549	9.768

seismic coefficient k_{max} cannot produce large sliding displacements compromising the stability/reliability of these slopes.

The sliding displacements in slopes with $\beta = 60^\circ$ are considerably higher than those in slopes with $\beta = 30^\circ$ due to their lower values of k_y. Thus, the sliding displacements in these slopes are more sensitive to the variations of maximum seismic coefficient k_{max} arising from the spatial variations of initial shear modulus. In general, the sliding displacement escalates as CoV_{G0} increases. Sliding displacements increase significantly as the correlation length increases to $\delta/H = 2$, and they change slightly at δ/H values higher than 2. For instance, deterministic sliding displacement D in the slope with $\beta = 60^\circ$ and $\mu_{G0} = 320$ MPa under earthquake shaking No. 3 is about 1.5 cm, while mean displacement μ_D is about 4 cm if initial shear modulus varies with CoV_{G0}=30% and $\delta/H = 2$ within the same slope model (see Fig. 12). This discrepancy between deterministic and stochastic sliding displacements is considerable and should be consistently addressed. Neglecting the spatial variability of initial shear modulus could lead to an unconservative estimation of sliding displacements especially in slopes subjected to ground motions with low values of PGA. Nonetheless, a smaller discrepancy between deterministic and stochastic sliding displacements can be seen in slopes subjected to the earthquake shakings with high levels of PGA (see Fig. 12).

Figures 13 and 14 compare the effects of variation of initial shear modulus on the maximum seismic coefficient in slopes with $\beta = 30^\circ$ and $\beta = 60^\circ$. In all cases it can be observed that the increase in stochastic μ_{kmax} compared to the deterministic maximum seismic coefficient k_{maxd} is considerably higher for the slopes inclined at $\beta = 30^\circ$ than for the slopes with $\beta = 60^\circ$. Although it is difficult to perceive this complex phenomenon, this discrepancy could be due to the effects of topographic irregularities and soil stratigraphy on the dynamic response of slopes and the level of contribution of these factors to total amplification. According to previous studies in the literature (e.g., Ashford *et al*., 1997; Bouckovalas and Papadimitriou, 2005), it is believed that the topographic amplification, in general, is more significant in slopes inclined at 60° than in slopes with $\beta = 30^\circ$ where the stratigraphic amplification might play a more important role in total dynamic response. Hence, in slopes with $\beta = 30^\circ$, the variations in stratigraphic amplification arising from the random heterogeneity of shear wave velocity might lead to remarkable changes in the total dynamic response of sliding mass and to correspondingly higher maximum seismic coefficients compared to those in slopes with an inclination of 60°. In most cases, at δ/H ratios lower than the critical value (i.e., $\delta/H = 2$), μ_{kmax}/k_{maxd} does not change considerably with the slope inclination, whereas the variations of μ_{kmax}/k_{maxd} with slope angle are significant at $\delta/H = 2$. As an example, for the slope model with μ_{G0}=320 MPa subjected to earthquake shaking No. 3, the ratio μ_{kmax}/k_{maxd} regarding $CoV_{G0} = 30\%$ and $\delta/H = 2$ increases from 1.15 to 1.48 if β decreases from 60° to 30°, while the decrease in β does not lead to a remarkable change in μ_{kmax}/k_{maxd} at $\delta/H = 0.2$ (see Fig. 14).

5 Probabilistic interpretation

Since the seismic sliding displacements play a vital role in the stability of slopes, estimating the probability that computed sliding displacement resulting from each set of probabilistic parameters is greater than deterministic sliding displacement is of interest. A high likelihood indicates that the spatial variation of initial shear modulus within the soil leads to a high discrepancy between stochastic and deterministic sliding displacement, and accordingly, neglecting the spatial variability of initial shear modulus results in an unconservative evaluation of sliding displacements.

Figure 15 compares the actual and lognormal cumulative probability distributions of estimated displacements. It can be observed that lognormal cumulative distribution function (CDF) represents the cumulative frequency of computed displacements reasonably well. Thus, the probability that computed sliding displacement corresponding to a set of statistical parameters is higher than the deterministic value can be calculated by

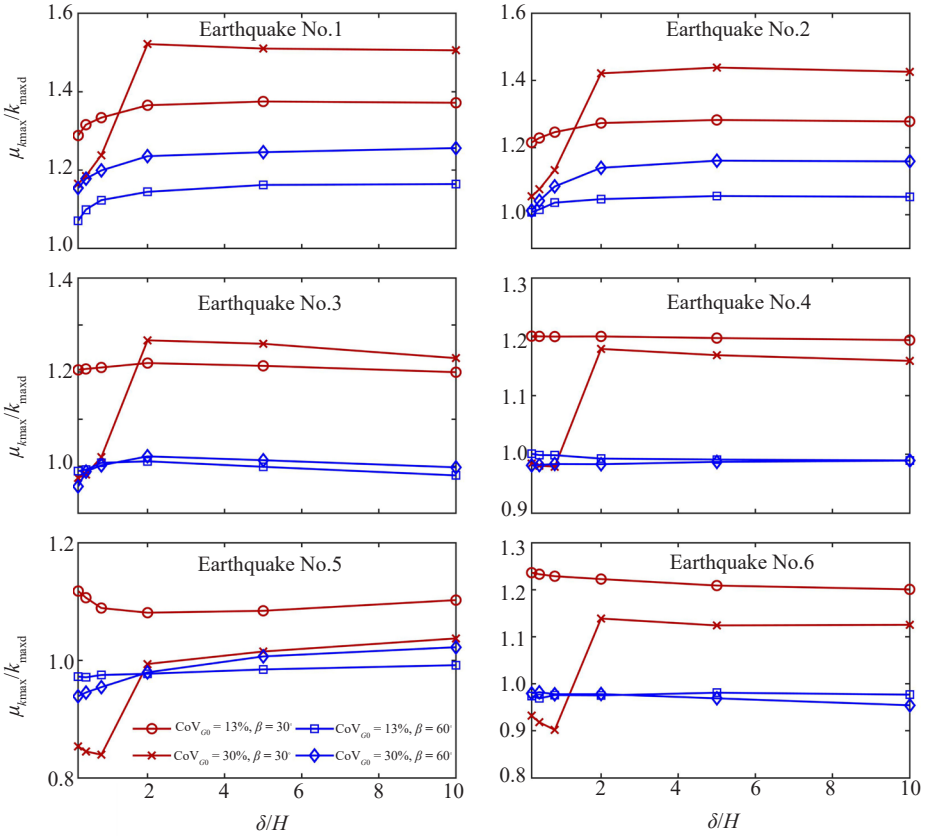

Fig. 13 The ratio between stochastic (mean) and deterministic maximum seismic coefficient as a function of β, CoV$_{G0}$ and δ/H for the slope model with μ_{G0} = 125 MPa

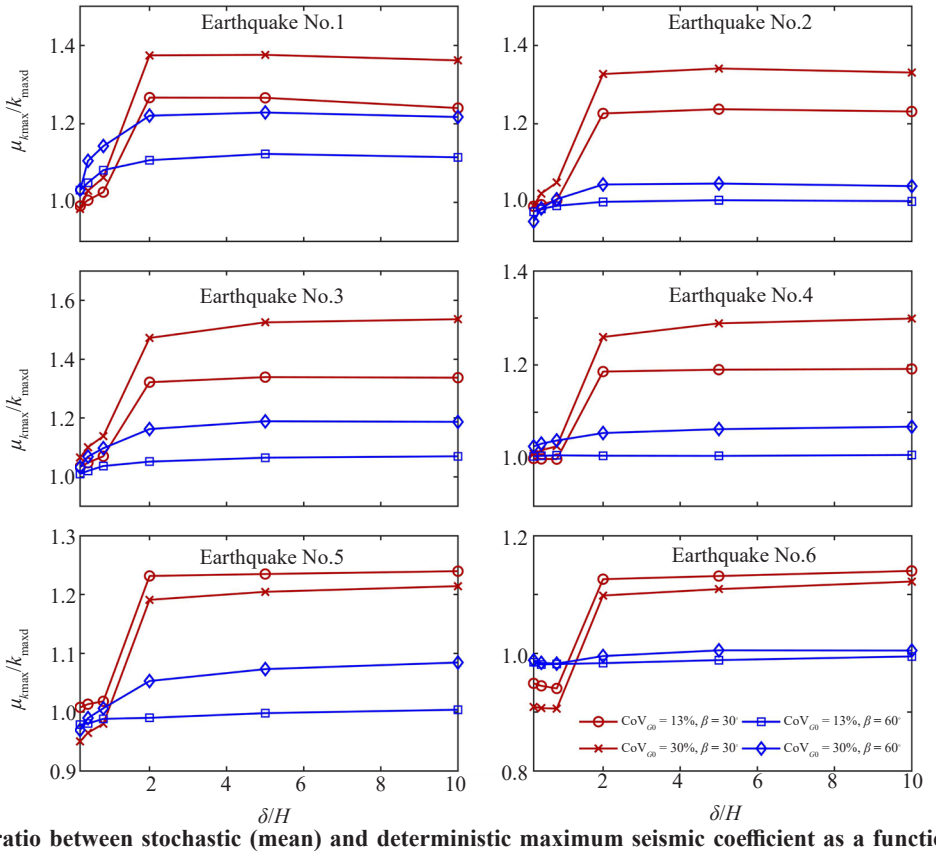

Fig. 14 The ratio between stochastic (mean) and deterministic maximum seismic coefficient as a function of β, CoV$_{G0}$ and δ/H for the slope model with μ_{G0} = 320 MPa

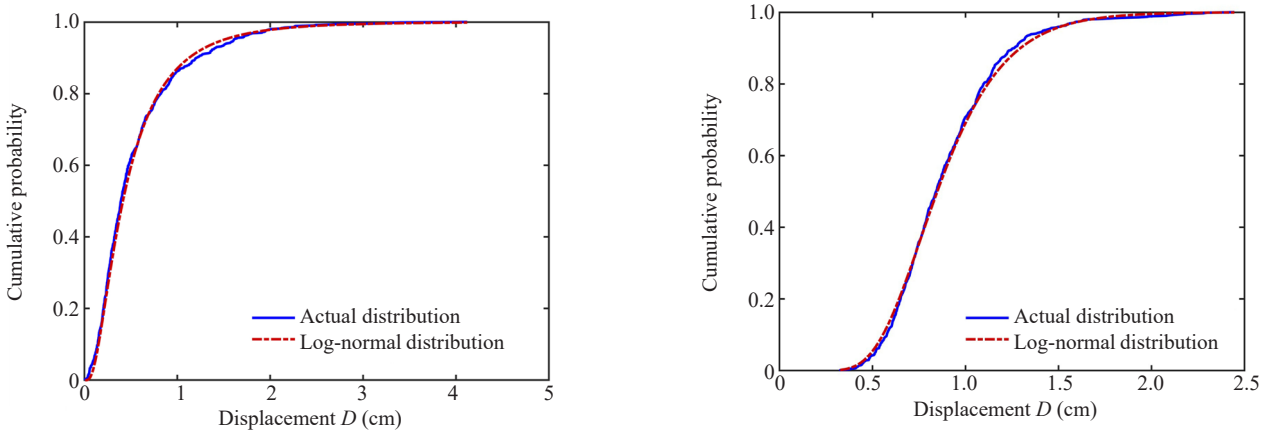

Fig. 15 Actual and lognormal cumulative probability distributions of estimated displacement associated with (a) earthquake No.1, μ_{G0} = 125 MPa, β = 60°, CoV$_{G0}$ = 30% and δ/H = 0.8 (b) earthquake No.2, μ_{G0} = 320 MPa, β = 60°, CoV$_{G0}$ = 13% and δ/H = 0.2

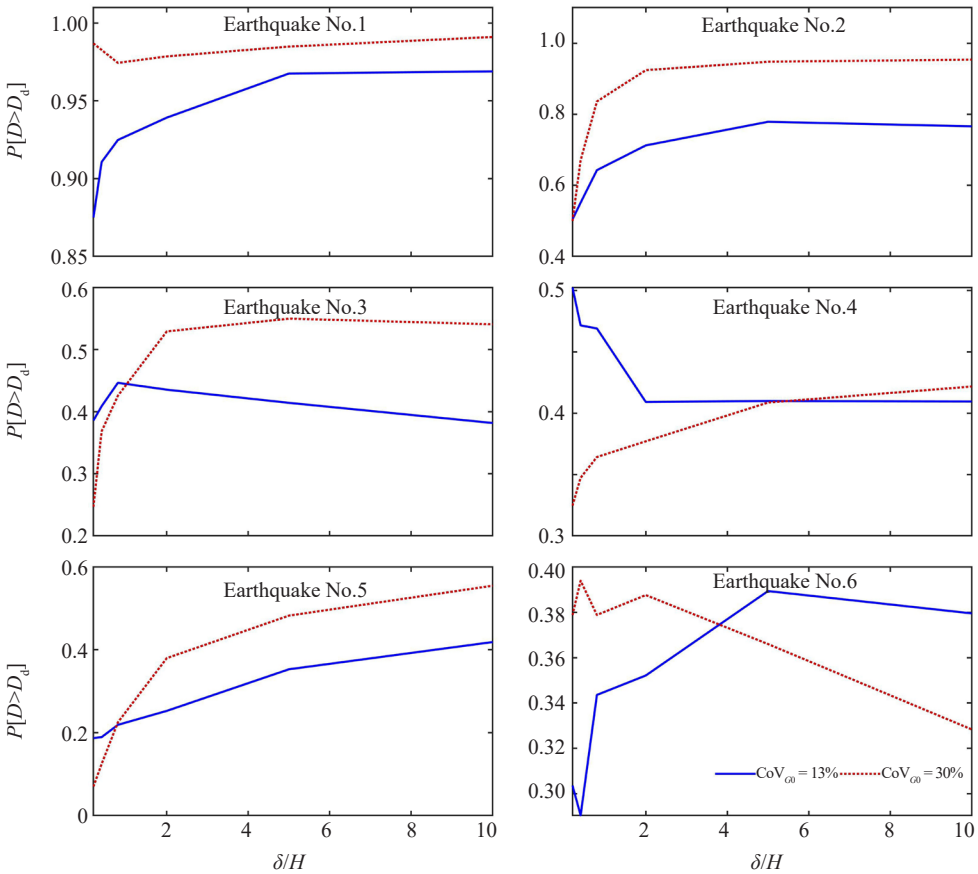

Fig. 16 Probability that estimated stochastic displacement for slope with β = 60° and μ_{G0} = 125 MPa is higher than the deterministic one

$$P[D> D_{\mathrm{d}}] = \Phi\left(\frac{\ln D_{\mathrm{d}} - \mu_{\ln D}}{\sigma_{\ln D}}\right) \tag{13}$$

where Φ is normal cumulative function, and D_{d} stands for the deterministic sliding displacement.

Figures 16 and 17 indicate how the probability $P[D>D_{\mathrm{d}}]$ changes with statistical parameters in slopes inclined at β = 60°. It can be observed that $P[D>D_{\mathrm{d}}]$ escalates as CoV$_{G0}$ increases, revealing that the presence of stiffer elements within the slope model results in higher stochastic displacements compared to deterministic ones as a result of higher maximum seismic coefficients. For example, in the slope with β = 60° and μ_{G0} = 125 MPa

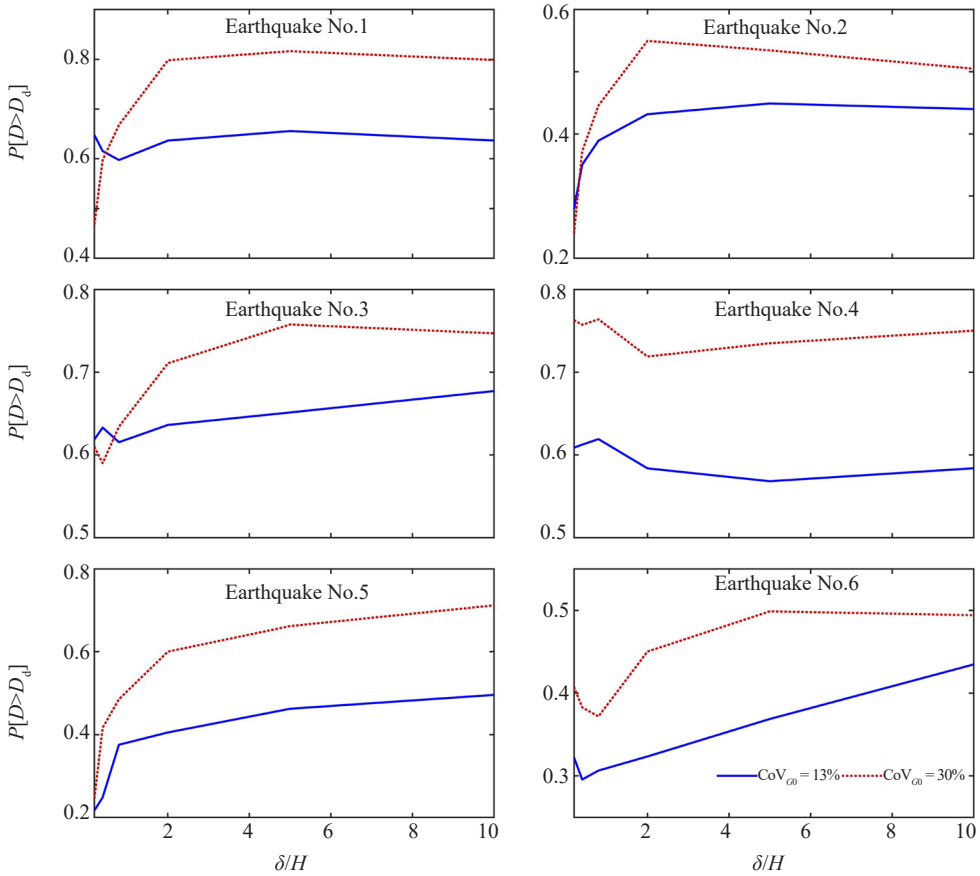

Fig. 17 Probability that estimated stochastic displacement for slope with β = 60° and μ_{G0} = 320 MPa is higher than the deterministic one

subjected to earthquake shaking No. 2, P[D>D_d] = 0.7 if CoV$_{G0}$=13% and δ/H = 2, whereas it increases to 0.91 at the same value of δ/H if CoV$_{G0}$ escalates to 30% (see Fig. 16). Moreover, $P[D>D_d]$ varies more significantly at higher ratios of δ/H (at critical or higher correlation lengths). It implies that the presence of stiffer elements further from softer ones brings about higher maximum seismic coefficients leading to a higher $P[D>D_d]$.

In general, the probability $P[D>D_d]$ is considerably lower for higher levels of PGA. It shows that the spatial variability of initial shear modulus in slopes subjected to ground motions with higher values of PGA has a lower impact on the seismic response of sliding mass, and as a result, it has a minimal effect on seismic sliding displacements in these slopes.

6 Conclusion

A numerical study into the effect of spatial variability of shear wave velocity on the seismic response of sliding mass and seismic sliding displacements has been carried out. The random fields of initial shear modulus were generated by employing Monte Carlo simulations in conjunction with the correlation matrix decomposition method. Subsequently, the dynamic analyses were performed from which the following conclusions could be drawn.

In general, the maximum seismic coefficients and sliding displacements increase with an increase in CoV$_{G0}$ and δ/H, since the presence of stiffer elements having higher shear modulus within the slope results in higher dynamic responses of sliding mass and accordingly higher sliding displacements. It indicates that stiffer elements dominate the total dynamic response of sliding mass.

The impact of spatial variability of shear wave velocity on the seismic response of sliding mass in slopes subjected to earthquake shakings with lower levels of PGA is more pronounced. In these cases, an escalation in δ/H from the values less than the critical value to the values equal to or higher than the critical value leads to a substantial increase in maximum seismic coefficient. Therefore, neglecting the spatial variability of shear wave velocity, in these cases, could lead to an unconservative estimation of sliding displacements.

The results reveal the fact that spatial variability of shear wave velocity leads to a higher increase in maximum seismic coefficients in slopes with the angle β = 30° compared to those in slopes inclined at β = 60°.

References

Ashford SA, Sitar N, Lysmer J and Deng N (1997), "Topographic Effects on the Seismic Response of Steep Slopes," *Bulletin of the Seismological Society of America*, **87**(3): 701–709.

Baecher GB and Christian JT (2003), *Reliability and Statistics in Geotechnical Engineering*, Wiley: Chichester, UK; Hoboken, NJ.

Berkane HD, Harichane Z, Çelebi E and Elachachi SM (2019), "Site Dependent and Spatially Varying Response Spectra," *Earthquake Engineering and Engineering Vibration*, **18**(3): 497–509. https://doi.org/10.1007/s11803-019-0517-6.

Bouckovalas GD and Papadimitriou AG (2005), "Numerical Evaluation of Slope Topography Effects on Seismic Ground Motion," *Soil Dynamics and Earthquake Engineering*, **25**(7): 547–558. https://doi.org/10.1016/j.soildyn.2004.11.008.

Bray JD and Rathje EM (1998), "Earthquake-Induced Displacements of Solid-Waste Landfills," *Journal of Geotechnical and Geoenvironmental Engineering*, **124**.

Cherubini C (2000), "Reliability Evaluation of Shallow Foundation Bearing Capacity on c'-ϕ' Soils," *Canadian Geotechnical Journal*, **37**: 264–269. https://doi.org/10.1139/t99-096.

Deng ZP, Li DQ, Qi XH, Cao ZJ and Phoon KK (2017), "Reliability Evaluation of Slope Considering Geological Uncertainty and Inherent Variability of Soil Parameters," *Computers and Geotechnics*, **92**: 121–131. https://doi.org/10.1016/j.compgeo.2017.07.020.

Der Kiureghian A and Ke JB (1988), "The Stochastic Finite Element Method in Structural Reliability," *Probabilistic Engineering Mechanics Journal*, **3**(2): 83–91. https://doi.org/10.1016/0266-8920(88)90019-7.

Gerolymos N, Escoffier S, Gazetas G and Garnier J (2009), "Numerical Modeling of Centrifuge Cyclic Lateral Pile Load Experiments," *Earthquake Engineering and Engineering Vibration*, **8**(1): 61–76. 10.1007/s11803-009-9005-8.

Griffiths DV and Fenton GA (2004), "Probabilistic Slope Stability Analysis by Finite Elements," *Journal of Geotechnical and Geoenvironmental Engineering*, **130**(5): 507–518. https://doi.org/10.1061/(ASCE)1090-0241(2004)130:5(507).

Griffiths DV, Fenton GA and Manoharan N (2002), "Bearing Capacity of Rough Rigid Strip Footing on Cohesive Soil: Probabilistic Study," *Journal of Geotechnical and Geoenvironmental Engineering*, **128**(9): 743–755. https://doi.org/10.1061/(ASCE)1090-0241(2002)128:9(743).

Griffiths DV, Huang J and Fenton GA (2009), "Influence of Spatial Variability on Slope Reliability Using 2-D Random Fields," *Journal of Geotechnical and Geoenvironmental Engineering*, **135**(10): 1367–1378. https://doi.org/ 10.1061/(ASCE)GT.1943-5606.0000099.

Gu Linlin, Ye Guanlin, Wang Zhen, Ling Xianzhang and Zhang Feng (2017), "Settlement Mechanism of Piled-Raft Foundation Due to Cyclic Train Loads and Its Countermeasure," *Earthquake Engineering and Engineering Vibration*, **16**(3): 499–511. https://doi.org/10.1007/s11803-017-0403-z.

Haldar S and Babu GLS (2008), "Effect of Soil Spatial Variability on the Response of Laterally Loaded Pile in Undrained Clay," *Computers and Geotechnics*, **35**(4): 537–547. https://doi.org/10.1016/j.compgeo.2007.10.004.

Hicks MA and Samy K (2002), "Influence of Heterogeneity on Undrained Clay Slope Stability," *Quarterly Journal of Engineering Geology and Hydrogeology*, **35**(1): 41–49. https://doi.org/10.1144/qjegh.35.1.41.

Huang Jingqi, Zhao Mi, Xu Chengshun, Du Xiuli, Jin Liu and Zhao Xu (2018), "Seismic Stability of Jointed Rock Slopes under Obliquely Incident Earthquake Waves," *Earthquake Engineering and Engineering Vibration*, **17**(3): 527–539. https://doi.org/10.1007/s11803-018-0460-y.

Hui Shuqing, Tang Liang, Zhang Xiaoyu, Wang Youqing, Ling Xianzhang and Xu Bown (2018), "An Investigation of the Influence of Near-fault Ground Motion Parameters on the Pile′s Response in Liquefiable Soil," *Earthquake Engineering and Engineering Vibration*, **17**(4): 729–745. https://doi.org/10.1007/s11803-018-0472-7.

Iran Institute of Earthquake Engineering and Seismology. http://www.iiees.ac.ir/en/.

Jamshidi CR, Davoodi M and Alinejad TA (2012), "Effects of Spatial Variability of Soil Properties on Natural Frequency of Natural Soil Deposits," *15th World Conference on Earthquake Engineering* (15WCEE), Lisbon, Portugal.

Jamshidi Chenari R and Aminzadeh Bostani Taleshani S (2016), "Site Response of Heterogeneous Natural Deposits to Harmonic Excitation Applied to More Than 100 Case Histories," *Earthquake Engineering and EngineeringVibration*, **15**(2): 341–356. https://doi.org/10.1007/s11803-016-0326-0.

Kim HK and Santamarina JC (2017), "Spatially Varying Small-Strain Stiffness in Soils Subjected to K_0 Loading," *KSCE Journal of Civil Engineering*, **22**(4): 1101–1108. https://doi.org/10.1007/s12205-017-0547-4.

Konai S, Sengupta A and Deb K (2018), "Behavior of Braced Excavation in Sand under a Seismic Condition: Experimental and Numerical Studies," *Earthquake Engineering and Engineering Vibration*, **17**(2): 311–324. https://doi.org/10.1007/s11803-018-0443-z.

Kuhlemeyer RL and Lysmer J (1973), "Finite Element

Method Accuracy for Wave Propagation Problems," *Journal of Soil Mechanics and Foundations Division*, **99**: 421–427.

Li L and Chu X (2016), "Effect of 2-D Random Field Discretization on Failure Probability and Failure Mechanism in Probabilistic Slope Stability," *Geotechnical and Geological Engineering*, **34**(2): 437–447. https://doi.org/10.1007/s10706-015-9955-8.

Liu LL, Cheng YM and Zhang SH (2017), "Conditional Random Field Reliability Analysis of a Cohesion-Frictional Slope," *Computers and Geotechnics*, **82**: 173–186. https://doi.org/10.1016/j.compgeo.2016.10.014.

Liu Qijian, Wu Zhiyu and Lee VW (2019), "Scattering and Reflection of SH Waves around a Slope on an Elastic Wedged Space," *Earthquake Engineering and Engineering Vibration*, **18**(2): 255–266. https://doi.org/10.1007/s11803-018-0472-7.

Lizarraga HS and Lai CG (2014), "Effects of Spatial Variability of Soil Properties on the Seismic Response of an Embankment Dam," *Soil Dynamics and Earthquake Engineering*, **64**: 113–128. https://doi.org/10.1016/j.soildyn.2014.03.016.

Low BK, Lacasse S and Nadim F (2007), "Slope Reliability Analysis Accounting for Spatial Variation," *Georisk: Assessment and Management of Risk for Engineered Systems and Geohazards*, **1**(4): 177–189. https://doi.org/10.1080/17499510701772089.

Makdisi F and Seed H (1978), "Simplified Procedure for Estimating Dam and Embankment Earthquake-Induced Deformations," *Journal of Geotechnical Engineering Division*, **104**(7): 849–867.

Metya S and Bhattacharya G (2016), "Reliability Analysis of Earth Slopes Considering Spatial Variability," *Geotechnical and Geological Engineering*, **34**(1): 103–123. https://doi.org/10.1007/s10706-015-9932-2.

Michael M, Al-Bittar T and Soubra AH (2016), "Effect of Soil Spatial Variability on the Dynamic Behavior of a Slope," *VII European Congress on Computational Methods in Applied Sciences and Engineering*, Crete Island, Greece.

Nadi B, Askari F and Farzaneh O (2014), "Seismic Performance of Slopes in Pseudo-Static Designs with Different Safety Factors," *Iranian Journal of Science and Technology*, **38**.

Nadi B, Askari F and Farzaneh O (2016), "Uncertainty in Determination of Seismic Yield Coefficient of Earth Slopes," *Bulletin of Earthquake Science and Engineering*, **2**(4): 47–54.

Nadi B, Askari F, Farzaneh O, Fatolahzadeh S and Mehdizadeh R (2019), "Reliability Evaluation of Regression Model for Estimating Co-Seismic Landslide Displacement," *Iranian Journal of Science and Technology, Transactions of Civil Engineering*, 1–9. doi: 10.1007/s40996-019-00247-1.

Newmark NM (1965), "Effect of Earthquakes on Dams and Embankments," *Geotechnique*, **15**(2):139–160.

Phoon KK and Kulhawy FH (1999), "Characterization of Geotechnical Variability," *Canadian Geotechnical Journal*, **36**(4): 612–624. https://doi.org/10.1139/t99-038.

Rathje EM and Antonakos G (2010), "A Unified Model for Predicting Earthquake-induced Sliding Displacements of Rigid and Flexible Slopes," *Engineering Geology*, **122**(1): 51–60. https://doi.org/10.1016/j.enggeo.2010.12.004.

Rathje EM, Abrahamson NA and Bray JD (1998), "Simplified Frequency Content Estimates of Earthquake Ground Motions," *Journal of Geotechnical and Geoenvironmental Engineering*, **124**(2): 150–159. https://doi.org/10.1061/(ASCE)1090-0241(1998)124:2(150).

Rathje EM and Saygili G (2011), "Estimating Fully Probabilistic Seismic Sliding Displacements of Slopes from a Pseudoprobabilistic Approach," *Journal of Geotechnical and Geoenvironmental Engineering*, **137**(3). https://doi.org/10.1061/(ASCE)GT.1943-5606.0000431.

Rizzitano S, Biondi G and Cascone E (2010), "Effect of Simple Topographic Irregularities on Site Seismic Response," *Proceedings of the Geotechnical Conference*, Dhaka, Bangladesh.

Sivakumar Babu GL and Mukesh MD (2003), "Risk Analysis of Landslides-A Case Study," *Geotechnical and Geological Engineering*, **21**(2): 113–127. https://doi.org/10.1023/A:1023525002893.

Tang Liang, Maula BH, Ling Xianzhang and Su Lei (2014), "Numerical Simulations of Shake-table Experiment for Dynamic Soil-Pile-Structure Interaction in Liquefiable Soils," *Earthquake Engineering and Engineering Vibration*, **13**(1): 171–180. https://doi.org/10.1007/s11803-014-0221-5.

Tang Liang, Zhang Xiaoyu, Ling Xianzhang, Li Hui and Ju Nengpan (2016), "Experimental and Numerical Investigation on the Dynamic Response of Pile Group in Liquefying Ground," *Earthquake Engineering and Engineering Vibration*, **15**(1): 103–114. https://doi.org/10.1007/s11803-016-0308-2.

Tang Liang, Cong Shengyi, Ling Xianzhang and Ju Nengpan (2017), "The Boundary Conditions for Simulations of a Shake-Table Experiment on the Seismic Response of 3D Slope," *Earthquake Engineering and Engineering Vibration*, **16**(1): 23–32. https://doi.org/10.1007/s11803-016-0308-2.

Tietje O, Fitze P and Schneider HR (2014), "Slope Stability Analysis Based on Autocorrelated Shear Strength Parameters," *Geotechnical and Geological Engineering*, **32**(6): 1477–1483. https://doi.org/10.1007/s10706-013-9693-8.

Zhang B, Li Y, Fantuzzi N, Zhao Y, Liu Y-B, Peng B and

Chen J (2019), "Investigation of the Flow Properties of CBM Based on Stochastic Fracture Network Modeling," *Materials* (*Basel*), **12**(15): 2387.

Zhang J, Cui P, Zhang B, Yang C and McVerry G (2010), "Earthquake-induced Landslide Displacement Attenuation Models and Application in Probabilistic Seismic Landslide Displacement Analysis," *Earthquake Engineering and Engineering Vibration*, **9** (2): 177–187. http://doi.org/10.1007/s11803-010-0004-6.

Notation

A = amplification factor

$a_i(t)$ = acceleration time history at each bottom-center point i located on the slip surface

B = thickness of the slope's foundation

C = correlation matrix

CoV_D = coefficient of variation of sliding displacement

$\mathrm{CoV}_{k\mathrm{max}}$= coefficient of variation of maximum seismic coefficient

CoV_{G0}= coefficient of variation of initial shear modulus

D = sliding displacement

D_d = deterministic sliding displacement

f_max= maximum frequency of input motion

G_0 = initial shear modulus

$G(x_i)$ = normal standard random field of initial shear modulus

$G_{0\mathrm{i}}$= lognormal random field of initial shear modulus.

H = height of slope

$k(t)$ = seismic coefficient time history

k_max = maximum seismic coefficient

k_maxd = deterministic maximum seismic coefficient

k_y= yielding acceleration

m_i = mass of ith block in sliding mass

M = magnitude of earthquake

PGA = peak ground acceleration

T_s = natural period of sliding mass

T_m = mean period of input motion

V_s = shear wave velocity

y = maximum depth of sliding mass

β = inclination of slope

δ = correlation length of initial shear modulus

Δl = maximum length of elements in the finite-difference mesh

ξ = Rayleigh damping ratio

$\mu_{\ln G0}$ = mean of log initial shear modulus

$\mu_{k\mathrm{max}}$= mean maximum seismic coefficient

μ_D= mean sliding displacement

μ_{G0}= mean initial shear modulus

ρ = correlation coefficient

σ_{G0}= standard deviation of initial shear modulus

$\sigma_{\ln G0}$= standard deviation of log initial shear modulus

τ = distance between any two points of the desired random field

Φ = normal cumulative function